Cent. Eur. J. Phys. • 9(2) • 2011 • 338-343
DOI: 10.2478/s11534-010-0107-8

VERSITA

Central European Journal of **Physics**

Optical and microstructural properties of self-assembled InAs quantum structures in silicon

Research Article

Sławomir Prucnal[1*], Marcin Turek[1†], Andrzej Drozdziel[1], Krzysztof Pyszniak[1], Artur Wójtowicz[1], Sheng-Qiang Zhou[2], Alohe Kanjilal[2], Artem Shalimov[2], Wolfgang Skorupa[2], Jerzy Zuk[1]

1 *Maria Curie-Skłodowska University, Pl. M. Curie-Skłodowskiej 1, 20-031 Lublin, Poland*

2 *Institute of Ion Beam Physics and Materials Research, Forschungszentrum Dresden-Rossendorf, P.O. Box 510119, 01314 Dresden, Germany*

Received 24 July 2010; accepted 13 October 2010

Abstract: The InAs quantum structures were formed in silicon by sequential ion implantation and subsequent thermal annealing. Two kinds of crystalline InAs nanostructures were successfully synthesized: nanodots (NDs) and nanopyramids (NPs). The peaks at 215 and 235 cm^{-1}, corresponding to the transverse optical (TO) and longitudinal optical (LO) InAs single-phonon modes, respectively, are clearly visible in the Raman spectra. Moreover, the PL band at around 1.3 μm, due to light emission from InAs NDs with an average diameter 7 ± 2 nm, was observed. The InAs NPs were found only in samples annealed for 20 ms at temperatures ranging from 1000 up to 1200°C. The crystallinity and pyramidal shape of InAs quantum structures were confirmed by HRTEM and XRD techniques. The average size of the NPs is 50 nm base and 50 nm height, and they are oriented parallel to the Si (001) planes. The lattice parameter of the NPs increases from 6.051 to 6.055 Å with the annealing temperature increasing from 1100 to 1200°C, due to lattice relaxation. Energy dispersive spectroscopy (EDS) shows almost stoichiometric composition of the InAs NPs.

PACS (2008): 81.40.Tv, 78.55.Cr, 78.67.Hc

Keywords: InAs • nanodots • nanopyramids • flash lamp annealing • photoluminescence

© *Versita Sp. z o.o.*

1. Introduction

Silicon is the most useful material in semiconductor electronics, but with its indirect band gap is a poor light emitter that reduces the field of its potential application. The optical properties of silicon can be easily improved by formation of optically active centers in silica or silicon matrices. Nowadays, devices such as light-emitting diodes (LED) [1], non-volatile memories [2], or solar cells [3] have been fabricated based on silicon nanocrystals embedded in silicon dioxide or silicon nitride films. Quantum dots (QDs) are, in particular, promising candidates for novel optoelectronic devices, like QD lasers, QD infrared pho-

*E-mail: s.prucnal@fzd.de
†E-mail: mturek@kft.umcs.lublin.pl (Corresponding author)

Springer

todetectors, single-photon emitters, etc. From the optical point of view, the QDs are interesting due to possibility of tuning the light emission by a quantum confinement size effect (QCSE), which modifies the bulk electronic band structure [4]. This effect is responsible for a size-dependent shift both in the optical band gap and in the exciton binding energy when the size of the particle R is of the order of the excitonic Bohr radius a_b [5, 6]. In the case of Si nanocrystals embedded in silica, the emission wavelength due to QCSE can be tuned in the range of about 500-1100 nm. Even broader spectral ranges can be expected from QDs based on $A_{III}B_V$ semiconductors embedded in different hosts. Such systems, depending on the particular matrix, can be used as efficient light emitters covering the spectrum from UV (AlN, GaN, ZnO) up to infrared (GaAs, InAs, InSb) [7]. The key problem for the wide application of the III-V QDs is their integration with silicon technology. The main fabrication methods for such QDs are: porous glass method [8], vapour deposition [9], radio frequency co-sputtering [10], sol-gel synthesis [11], and ion implantation [12]. Recently, different QDs made of $A_{III}B_V$ or $A_{II}B_{VI}$ semiconductor compounds have been synthesised in silicon or in its oxide layer by ion implantation and subsequent thermal annealing [13, 14].

The main problems that appear during such QD preparation process are thermal diffusion of the implanted elements and large size deviations of the QDs. In this paper we present a method of producing QDs that are homogeneously distributed in the hosts and have small deviations in size. The main problem – the thermal diffusion of implanted elements during annealing – was solved by introducing the flash lamp annealing (FLA) technique into preparation steps of the QDs. The standard annealing time for FLA varies from 0.8 to 20 ms. On one hand, the thermal budget of energy absorbed by a sample during the flash is sufficient to out-anneal defects introduced to the sample during ion implantation and activate QDs formation. On the other hand, the annealing time is too short for out-diffusion of dopants introduced into the sample. The detailed study of the influence of the annealing conditions on the optical and structural properties of the InAs QDs reveals that after long annealing time, at least for a few minutes, only spherical InAs nanocrystals, called nanodots (NDs), are formed in the silicon or SiO_2 matrix. Moreover, most of the indium diffuses out of the sample and starts to accumulate on the sample surface as kind of small crystallites. After 20 ms FLA annealing at a temperature above 1000°C, besides small InAs NDs (average diameter 7 ± 2 nm), the pyramidal shaped InAs nanostructures (NPs) were found. The structural properties of the InAs NPs and the growth mechanism are presented.

2. Experimental details

Single crystalline n-type (100) silicon wafers covered by a 100 nm thick thermally grown oxide layer were implanted sequentially with As and In ions. Initially, 170 keV As^+ ions were implanted with a fluence of 3.2×10^{16} ion/cm^2. The implantation was performed at 500°C in order to initiate the clustering process of arsenic during ion implantation. Subsequently, the samples were implanted by 240 keV In^+ ions with a fluence of 3×10^{16} cm^{-2} at room temperature. The expected impurity concentration is $5 \cdot 10^{21}$ cm^{-3} at a depth of ~ 120 nm. The distribution of the implanted ions was first calculated by the SRIM 2007 code and confirmed by Rutherford Backscattering Spectrometry (RBS). The RBS spectra were collected with a collimated 1.7 MeV He^+ beam at the backscattering angle of 170°. After the implantation the samples were annealed at different temperatures and times in order to estimate the most suitable annealing conditions for InAs QDs formation. Three different annealing techniques were employed: furnace annealing at temperatures ranging from 700 to 900°C for 30 min, rapid thermal annealing (RTA) in the same temperature range but with 30 s and 1 min annealing times, and flash lamp annealing (FLA) with 600°C preheating for 1 min and annealing temperatures ranging from 700 to 1200°C for 20 ms. In all cases samples were annealed in argon ambient. The optical properties were investigated by μ-Raman spectroscopy and low temperature photoluminescence. The μ-Raman spectra were recorded at room temperature with a backscattering geometry in the range of 150-600 cm^{-1} using a 532 nm YAG laser. The PL spectra were measured in the temperature range from 15 to 300 K using the Jobin Yvon Triax 550 monochromator and a cooled InGaAs detector. For the NDs excitation during PL measurements, the 532 nm laser light with a power of 20 mW was applied. Cross-sectional transmission electron microscopy images were taken by means of the FEI Titan 80-300 STEM operating at 300 keV. Lattice parameters and dimensions of InAs nanoparticles were determined at room temperature by means of synchrotron radiation X-ray diffraction (SRXRD) at the BM20 (ROBL) beamline at the European Synchrotron Radiation Facility (ESRF). Longitudinal $\frac{2\theta}{\omega}$ scans have been performed in a coplanar geometry using a parallel monochromatic beam with $\lambda = 1.54056$ Å wavelength.

3. Results and discussion

Fig. 1 shows the RBS spectra of the 'as implanted' and annealed samples at 1150 and 1200°C for 20 ms with 600 °C preheating for 1 min (FLA) and annealed at 850°C for

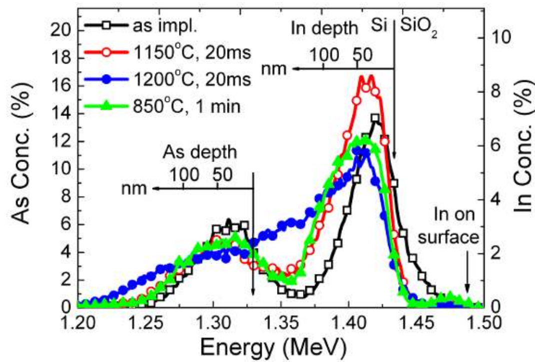

Figure 1. RBS spectra of the As- and In-implanted and annealed samples: (□) – 'as implanted', (▲) – 850°C, 1 min (RTA), (○) – 1150°C, 20 ms (FLA), (●) – 1200°C, 20 ms (FLA).

1 min (RTA). The RBS measurements performed at the FLA annealed samples with temperature up to 1100°C did not show diffusion of the implanted elements, or the amount of the impurities which diffuse during the annealing is below the RBS sensitivity (not shown here). The broadening of the As and In depth profiles is observed in the sample annealed at 1150°C for 20 ms or at a higher temperature. An increase of the annealing temperature up to 1200°C leads to relatively strong diffusion of both In and As into the depth of the silicon. The depth profile of arsenic is much broader (even in the 'as implanted' sample) than that predicted by SRIM code, due to the diffusion of arsenic during the hot implantation process. The hot implantation of arsenic was chosen to initiate the clustering process of As during ion implantation. The sample annealed at 850°C for 1 min exhibits not only diffusion of both elements into silicon but also strong out-diffusion of In atoms and their accumulation on the sample surface. In the case of the sample annealed in the furnace for 30 min for all temperatures, strong out-diffusion of both implanted elements was observed. After annealing at 900°C for 30 min, the concentration of indium is reduced to 20% of the total fluence, and big indium dots on the surface are visible. Moreover the sizes of the InAs NDs vary from a few to several tens of nanometers. Therefore, the FLA technique has a big advantage over RTA or furnace annealing (FA). The silicon matrix during ion bombardment becomes amorphous and recrystallizes after annealing. The speed of the recrystallization of silicon depends on annealing temperature, time, and crystallographic orientation of silicon. It was found that the impurities diffusion in silicon is directly connected with the recrystallization regrowth process of silicon (movement of the amorphous/crystalline (a/c) interface), and the recrystallization of silicon is due to solid-phase epitaxy regrowth (SPE) [15]. The a/c interface pushes the impurities, i.e. arsenic, to the surface. The amount of As that can be moved to the surface is inversely proportional to the regrowth speed of silicon. Moreover, the SPE is much faster than diffusion of As or In and increases with temperature much faster than diffusivity. Hence, after high temperature FLA (up to 1150°C) silicon is recrystallized, and no significant diffusion of the implanted elements is observed. Simultaneously, the thermal budget introduced to the sample during FLA is sufficient to create InAs quantum structures. The optical and microstructural properties of the InAs nanostructures were investigated by means of μ-Raman and photoluminescence spectroscopy. Figures 2a and 2b show the Raman spectra obtained from implanted and annealed samples. In the 'as implanted' sample we have observed two broad bands at 150 and 460 cm^{-1}. These bands are associated with defects in the SiO_2 layer, mainly broken bonds between oxygen atoms (-Si-O··O-Si-, dots mean broken bond) or highly elongated bonds that are created in silica during ion implantation [16, 17]. Moreover, the peak at 520 cm^{-1}, which is a fingerprint of the crystalline silicon, was not visible. That leads to the conclusion that the top layer of Si is fully amorphous. The broad bands at 150 and 460 cm^{-1} in the Raman spectra were detectable from the samples annealed at 700°C as well. For higher annealing temperature these bands disappear from Raman spectra due to reconstruction of broken bonds in silica. The annealing at 700°C or higher temperature leads to the recrystallization of the silicon layer, which manifests in the Raman spectra as a sharp peak at 520 cm^{-1} (see Fig. 2b). The sample annealed at 700°C even for 30 min and the 'as implanted' one did not show any evidence of InAs structure formation, neither crystalline nor amorphous. Two peaks at 216 and 235 cm^{-1}, due to transverse optical (TO) and longitudinal optical (LO) phonons in the InAs quantum structures, appear from samples annealed at 850°C or higher temperatures [18]. They are observed from samples annealed both for a longer time, and in the milliseconds range. In the case of FLA the InAs QDs start to grow at temperatures above 900°C. The best crystalline quality of the InAs NDs was obtained after annealing at 1150°C for 20 ms. It is worth noticing that in such a case, the InAs nanocrystals growth is by liquid-phase epitaxy. The average diameter of InAs NDs formed during FLA is about 7 ± 2 nm, and they are located on both sides of SiO_2/Si interface. Such nanocrystals can be efficiently excited. The photoluminescence spectra obtained from a sample annealed at 1150°C for 20 ms are presented in Fig. 3. Samples were excited with a green laser at 532 nm with

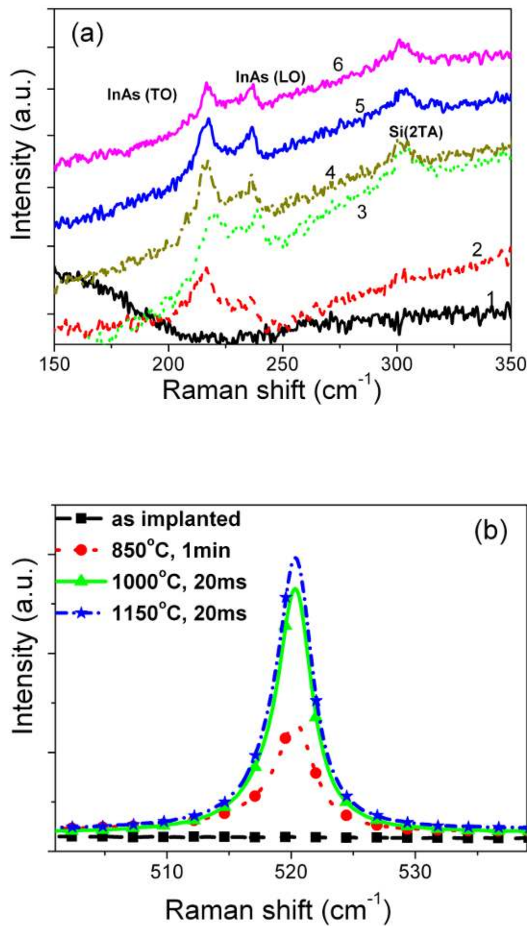

Figure 2. (a) Raman spectra of In- and As-implanted samples annealed at 850°C for 1 min (2) and at different temperatures range 20 ms (1000°C – (3), 1100°C – (4), 1150°C – (5), 1200°C – (6)). The as-implanted sample (1) is shown as well. Raman signal from crystalline silicon is shown on (b).

excitation power of 20 mW, and the sample temperature during excitation was changing from 15 to 300 K. The PL signal corresponding to the InAs NDs was detectable in the temperature range of 15-120 K. The narrow band at 1300 nm is related to crystalline InAs NDs with an average diameter of 7 ± 2 nm. The size of the InAs NDs was confirmed by the HRTEM investigation. Similar results, with some variation in the PL intensity, were obtained from other samples annealed at temperature ranging from 1000-1200°C for 20 ms. Besides the main InAs NDs luminescence, the small band at about 1530 nm was visible. This luminescence corresponds to defects, such as oxygen interstitials, existing in the silicon matrix. The low energy PL band around 1410 nm originates from the radiative recombination inside crystalline grains [19]. Moreover, the PL intensity drop around 1390 nm is due to water vapour absorption [20].

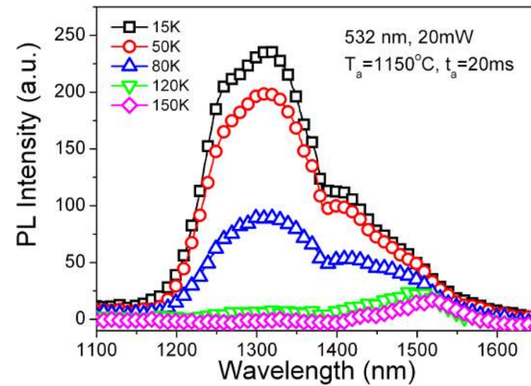

Figure 3. PL spectra recorded at different temperatures from sample at 1150°C for 20 ms. Sample was excited with 532 nm laser light.

The microstructural properties of the As- and In-implanted and annealed samples, investigated using bright-field HRTEM by keeping the electron beam along the [011]-zone axis, are presented in Fig. 4. Discernibly, the InAs nanocrystals are formed in the silicon matrix after RTA at 850°C for 1 min close to the SiO_2/Si interface, with the average size of 15 ± 3 nm, and they are randomly oriented (see Fig. 4a). Formation of the InAs nanocrystals after RTA was confirmed by μ-Raman spectroscopy as well (see Fig. 2a), where the transverse optical (TO) and longitudinal optical (LO) phonons of InAs were observed at about 215 and 235 cm^{-1}, respectively. Moreover, pyramidal or dome-shaped crystalline In nanostructures formed on the SiO_2 surface were observed (see the inset in Fig. 4a). The size and density of the In nanostructure are strongly dependent on the annealing time and temperature. The average size of the In nanopyramids obtained after annealing at 850°C for 1 min is 40 ± 10 nm, with a height of 20 ± 5 nm. After furnace annealing the size variation was much higher. Figures 4b and 4c show the InAs nanostructures formed by FLA at 1150 and 1200°C for 20 ms, respectively. Along with self-assembled and randomly oriented, small InAs nanocrystals with average diameter of 7 ± 2 nm in the SiO_2 layer, pyramidal crystalline InAs nanostructures in the silicon matrix were produced. The InAs NPs are grown vertically on the Si substrate, and they are formed between ⟨111⟩ - oriented twins. The Moiré pattern was observed in pyramidal InAs

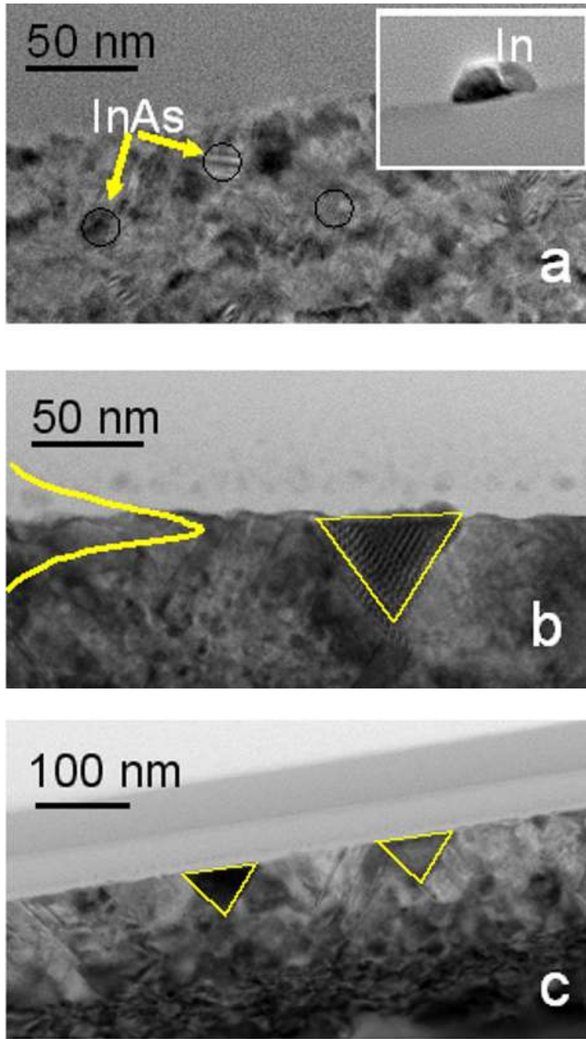

Figure 4. Bright field HRTEM micrographs of Si co-implanted by As and In followed by annealing at 850°C for 1 min (a), 1150°C for 20 ms (b) and 1200°C for 20 ms (c). Inset of Figure 4a shows In nanopyramid formed on the SiO_2 surface. The yellow line in Fig. 4b shows the RBS profile of In.

nanostructures. A corresponding HRTEM image confirms the formation of crystalline NPs (not shown). They are located close to the SiO_2/Si interface, around 2 nm below the interface. The sample annealed at 1150°C for 20 ms shows the NPs with average size of 45 nm. After annealing at 1100 or 1200°C, the average size of the InAs NPs changes about ±5 nm. Moreover, the formation of amorphous InAs nanodots in SiO_2 was observed when annealed at 1200°C. The depth profile of In obtained by RBS measurements from a sample annealed at 1150°C for 20 ms is also shown in Fig. 4b. We believe that

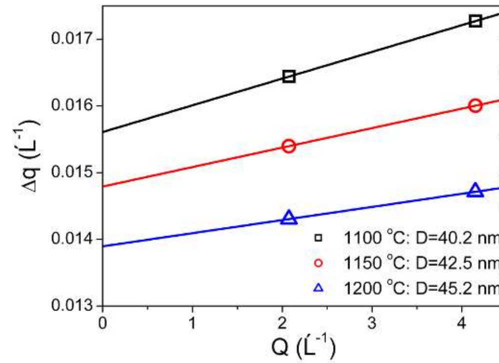

Figure 5. Williamson-Hall plot [21] for samples annealed at 1100, 1150, and 1200°C for 20 ms in reciprocal space units.

by properly controlling the preparation parameters (such as ion implantation fluence, annealing time and temperature) and introducing photolithography pre-patterning as an intermediate stage, it is possible to form well-aligned InAs nanopyramids with a defined size. The dimension of InAs nanoparticles for all samples were estimated using a Williamson-Hall plot in units of reciprocal space, where Δq corresponds to the FWHM of the peak in reciprocal space in the XRD spectrum (not shown here), while $\mathbf{Q}$ is related to the reciprocal lattice vector (see Fig. 5). The offset on the Δq-axis of the extrapolated linear dependence of $\Delta q(\mathbf{Q})$ is inversely proportional to the nanoparticle's dimension D, according to the relation

$$\Delta q(\mathbf{Q}=0)=\frac{2\pi}{D}.$$

The slope of the extrapolated line depends on the state of the internal strain of the particles. We have found that the average size of InAs inclusions increases from 40.2 nm up to 45.2 nm and grows with the annealing temperature, while the internal strains consequently decrease. These results are in good agreement with HRTEM measurements. The relative distortions of the InAs unit cell have been estimated according to the relation

$$\varepsilon=\frac{a_{\rm exp}-a_0}{a_0},$$

where $a_{\rm exp}$ and $a_0 = 6.0583$ Å are experimentally obtained and the table [22] lattice parameters of InAs, respectively. Lattice parameters of InAs nanoparticles, their average size and relative lattice distortion, are given in Table 1. The decrease of the relative distortion ε with growing annealing temperature is due to annealing out of defects and internal strains in crystalline InAs nanostructures.

Table 1. InAs lattice parameters (a_{exp}), nanoparticles dimension (D) and relative lattice distortion (ε).

Sample	a_{exp} (A)	D (nm)	ε (%)
1100°C	6.05182	40.2	-0.107
1150°C	6.05421	42.5	-0.068
1200°C	6.05543	45.2	-0.047

4. Conclusions

In summary, we have shown that the InAs quantum structures can be successfully produced by ion implantation and millisecond-range annealing. The FLA has a big advantage over other annealing techniques due to small size distribution of the QDs. Besides nanodots, the InAs nanopyramids were formed in the silicon matrix. The size of the NP can be easily controlled by modulation of the annealing temperature. The main advantage of the method used in this paper for InAs nanostructure formation is their integration with large-scale silicon technology, which allows application of the method to Si-based optoelectronic devices.

Acknowledgements

This work was partially supported by the Polish Ministry of Science and Higher Education, Grant No N N515 246637.

References

[1] J. Valenta, N. Lalic, J. Linnros, Appl. Phys. Lett. 84, 1459 (2004)

[2] J.H. Chen et al., Jpn. J. Appl. Phys. 46, 6586 (2007)

[3] X.J. Hao et al., Sol. Energy Mater. Sol. Cells 93, 273 (2009)

[4] L.E. Brus, J. Chem. Phys. 80, 4403 (1984)

[5] T. Canham, Appl. Phys. Lett. 57, 1046 (1990)

[6] S. Sapra, D.D. Sarma, Phys. Rev. B 69, 125304 (2004)

[7] J. Murphy, J.L. Coffer, Appl. Spectrosc. 56, 16A (2002)

[8] M.D. Dvorak, B.L. Justus, D.K. Daskill, D.G. Hendershot, Appl. Phys. Lett. 66, 804 (1995)

[9] T. Shmizu-Iwayama et al., J. Appl. Phys. 75, 7779 (1994)

[10] R. Ding et al., Mater. Chem. Phys. 76, 262 (2002)

[11] R.L. Wells, S.R. Aubuchon, S.S. Kher, M.S. Lube, Chem. Mater. 7, 793 (1995)

[12] A. Meldrum, L.A. Boatner, C.W. White, Nucl. Instrum. Meth. B 178, 7 (2001)

[13] F. Komarov et al., Nucl. Instrum. Meth. B 266, 3557 (2008)

[14] A.L. Tchebotareva, J.L. Brebner, S. Roorda, C.W. White, Nucl. Instrum. Meth. B 175-177, 187 (2001)

[15] K. Suzuki et al., IEEE Trans. Electron Devices 54, 262 (2007)

[16] G.E. Walter, P.N. Krishnan, S.W. Freiman, J. Appl. Phys. 52, 2832 (1981)

[17] Y. Hibino, H. Hanafusa, K. Ema, S. Hyodo, Appl. Phys. Lett. 47, 812 (1985)

[18] M.Yu. Ladanov et al., J. Exp. Theor. Phys. 101, 554 (2005)

[19] M. Yamaguchi, K. Morigaki, J. Phys. Soc. Jpn. 62, 2915 (1993)

[20] C.J. Patel, Q.X. Zhao, O. Nur, M. Willander, Appl. Phys. Lett. 72, 3047 (1998)

[21] G.K. Williamson, W.H. Hall, Acta Metall. 1, 22 (1953)

[22] M. Levinstein, S. Rumyantsev, M. Shur, Handbook Series on Semiconductor Parameters, vol. 2 (World Scientific, Singapore, 1996)